Studies of microwave radiation from a low-energy rotating electron beam in a multiresonator magnetron cavity

E. Chojnacki, W. W. Destler, W. Lawson, and W. Namkung[a)]
Electrical Engineering Department, University of Maryland, College Park, Maryland 20742

(Received 20 August 1986; accepted for publication 31 October 1986)

The generation of microwave radiation at high harmonics of the cyclotron frequency by a low-energy annular rotating electron beam (27 kV, 1 A, 3 μs) via interaction with the modes of a magnetron-type conducting boundary has been studied experimentally. Details of producing the axis-encircling E layer by magnetic cusp injection are presented. Narrow-band microwave radiation has been obtained from the device at power levels of 9.1 kW at 6.78 GHz (eighth cyclotron harmonic) and 2.2 kW at 8.85 GHz (tenth cyclotron harmonic). Measurements of the radiated power spectra and confining magnetic field have allowed identification of operating waveguide modes and instability mechanisms. An experimental comparison with respect to threshold beam power is presented between waveguide structures operating in the π mode and the 2π mode.

I. INTRODUCTION

In recent years there has been an active interest in the study of high-power microwave production from a variety of sources. This interest has resulted from possible applications of these sources to such diverse areas as high-power radar, rf heating of fusion plasmas, particle accelerators, and directed energy systems. Many concepts have been explored as potentially efficient sources of microwave and millimeter-wave radiation; these include gyrotrons,[1–3] free-electron lasers,[4–6] virtual cathode oscillators,[7,8] and relativistic adaptations of the magnetron[9,10] and backward-wave oscillator.[11,12]

At the University of Maryland, studies of the production of microwave radiation by cusp-injected rotating electron beams interacting with multiresonator magnetron circuits have been underway for several years.[13–18] These studies had followed naturally from observations of microwave radiation produced by negative mass unstable rotating electron beams in smooth cylindrical and coaxial waveguides.[19,20] The first experimental report that high-power microwaves could be efficiently produced by a rotating beam in a magnetron circuit device was in 1981 using a highly relativistic beam source (2 MeV, 2 kA).[13] Both theoretical and experimental work on this type of device have been pursued at several laboratories since that time.[21–25] The device has been called by several names, including Cusptron, Large Orbit Gyrotron, Gyromagnetron, and High Harmonic Gyrotron. Here, the term large orbit gyrotron is used with the tacit assumption that a cusp-injected beam is the most practical and efficient way to operate the device.

The primary reasons for interest in this configuration include the following: (a) radiation is produced at high harmonics (6–20) of the cyclotron frequency and therefore magnetic fields can be much lower than those required for small-orbit gyrotrons; (b) magnetic cusp injection requires a simple diode configuration for a beam source; (c) an axis-encircling annular beam is essentially devoid of the velocity shear present in a conventional magnetron; therefore, mode purity is easier to maintain with large numbers of resonators; and (d) the absence of radial electric fields associated with magnetrons allows electrons to move to smaller radii as they lose energy to radiation, making dc and rf breakdowns less likely and operation at high power and long pulse duration possible.

The first theoretical treatment of this specific device was reported by Lau and Barnett,[21] who argued that the device could operate at mildly relativistic electron energies. Operation of the device at low energy was confirmed in a report by Namkung[16] in which radiation was produced by a weakly relativistic rotating electron beam (17 keV, 1 A) at the sixth harmonic of the cyclotron frequency using a six-slot structure. The electronic efficiency was reported to be several percent. Additional low-energy theoretical work by Chu and Dialetis[23] has indicated that the beam current threshold for start oscillation of the device should be lower for the π mode than that for the 2π mode.

In this paper are described experiments performed on a low-energy device in which a rotating electron beam (20–30 keV, 1–2 A) interacts with ten- and twenty-slot multiresonator magnetron circuits. Measurements of output power spectra corresponding to various operating conditions are presented, including a comparison of devices designed to operate at the π mode and the 2π mode. These measurements will be compared with theoretical predictions. The generation of high-quality rotating electron beams via cusp injection is discussed in Sec. II. The theoretical design of the present device and the results of microwave experiments are presented in Sec. III. Conclusions are drawn in Sec. IV.

II. BEAM DYNAMICS

A. Theory

Extensive theoretical and experimental investigations of beam dynamics in cusp-injected systems have been reported elsewhere.[26–29] Presented here is a brief theoretical review.

If an electron is traveling in the positive z direction at radius r_0 in a uniform magnetic field upstream ($z<0$) of a magnetic cusp, conservation of kinetic energy and canonical angular momentum can be used to determine the orbit

[a)] Permanent Address: Naval Surface Weapons Center, Silver Spring, MD.

 0021-8979/87/041268-08$02.40

downstream of the cusp transition. Figure 1(a) shows an ideal step-function cusp transition at $z = 0$ where the downstream Larmor radius is given by

$$r_L = \frac{r_0}{2}\left(1 - \frac{B_1}{B_2}\right), \tag{1}$$

the guiding-center radius is

$$r_{gc} = |r_L - r_0|, \tag{2}$$

and the downstream axial velocity is

$$v_{z2} = \left[v_{z1}^2 - r_L^2(\Omega/\gamma)^2\right]^{1/2}. \tag{3}$$

Here B_1 and B_2 are the upstream and downstream magnetic fields, respectively, v_{z1} is the initial particle velocity, $\Omega = (eB_2)/m_0$ is the downstream nonrelativistic cyclotron frequency, and γ is the relativistic mass factor. The electron orbit in a transverse plane is shown in Fig. 1(b). If $B_1 = -B_2$, then $r_L = r_0$, $r_{gc} = 0$, and the downstream beam would be a perfectly uniform rotating cylinder.

A real cusp, however, has a finite transition width which gives rise to a finite guiding-center radius regardless of field magnitudes. Modeling the cusp field in the balanced ($B_1 = -B_2$) case as

$$B_z = -B_0 \tanh(z/\zeta), \tag{4}$$

the minimal downstream guiding-center radius becomes

$$r_{gc} = (\zeta/2)\sin^{-1}(1/\eta), \tag{5}$$

where ζ is a measure of the field transition width and $\eta = v_{z1}\gamma/r_0\Omega$. The field shape of Eq. (4) and resulting orbit is shown in Fig. 2. This effect of a minimal guiding-center

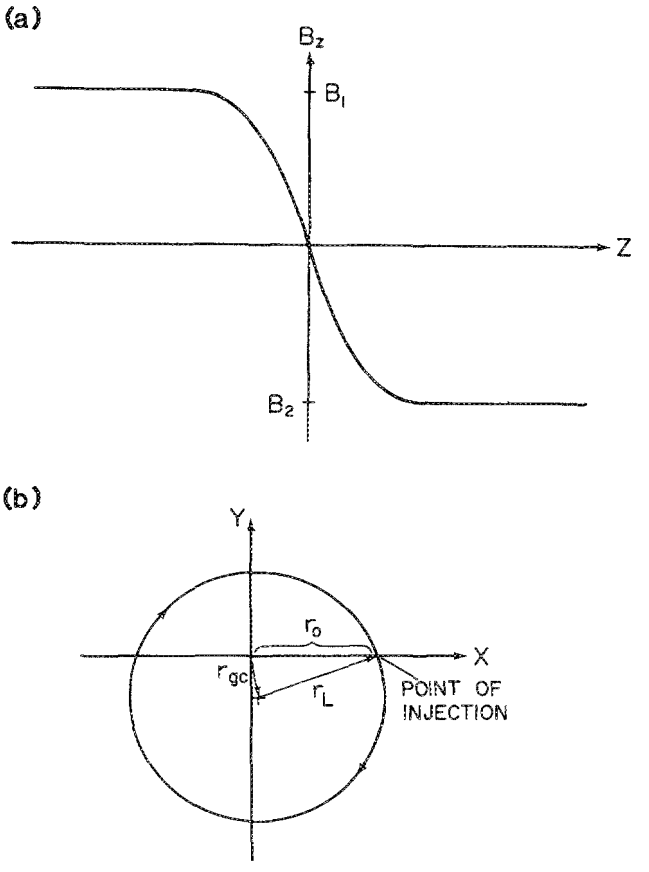

FIG. 2. (a) Realistic cusp transition of Eq. (4) and (b) the resulting electron orbit.

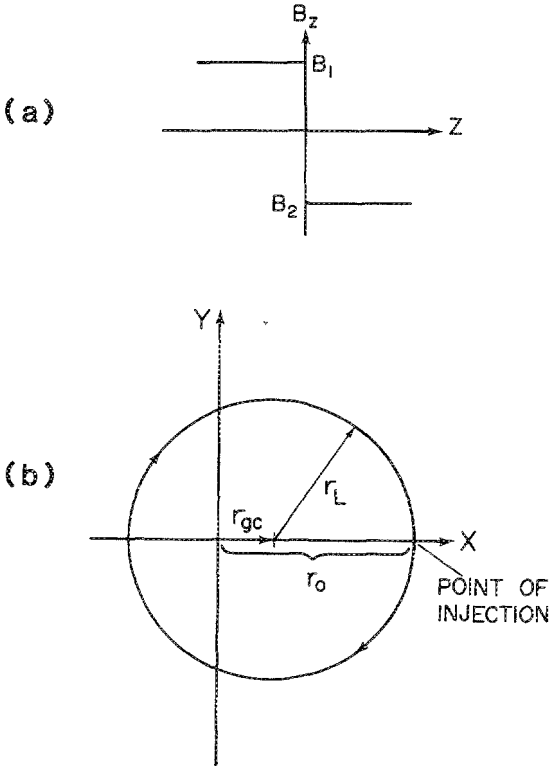

FIG. 1. (a) Ideal step-function magnetic cusp at $z = 0$ and (b) the corresponding electron orbit in a transverse plane.

radius has been termed "coherent off-centering" since all particles in an annular beam perform this orbit in phase, resulting in a scalloped beam envelope downstream (Fig. 3). The scallop wavelength is given by

$$\lambda = 2\pi r_0(\eta^2 - 1)^{1/2}. \tag{6}$$

B. Experiment

The experimental configuration used to produce a rotating E layer is shown in Fig. 4. The basic beam-injection scheme is modeled after the high-power Rotating Beam Facility at the University of Maryland.[16,26]

A magnetic cusp is formed by opposing solenoids with a soft iron plate placed in between to narrow the cusp transition width. The iron plate has an annular slot centered on axis to allow passage of the electron beam. An axially

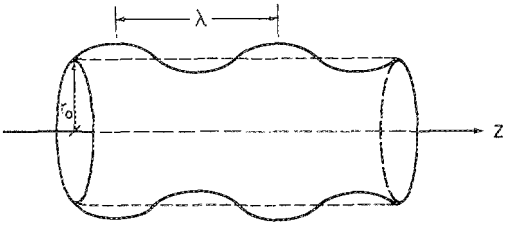

FIG. 3. Scalloped downstream beam envelope resulting from coherent off-centering.

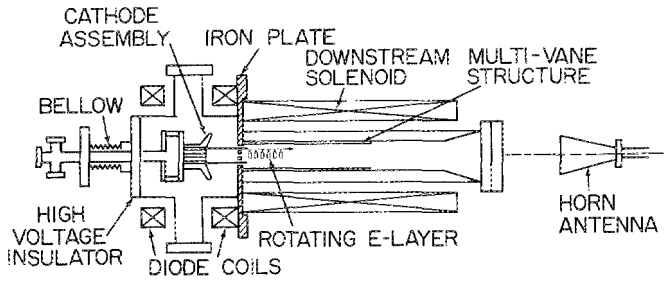

FIG. 4. Experimental configuration used to produce a rotating E layer and microwave radiation.

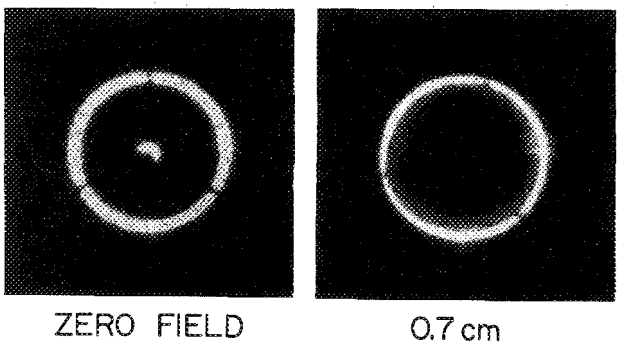

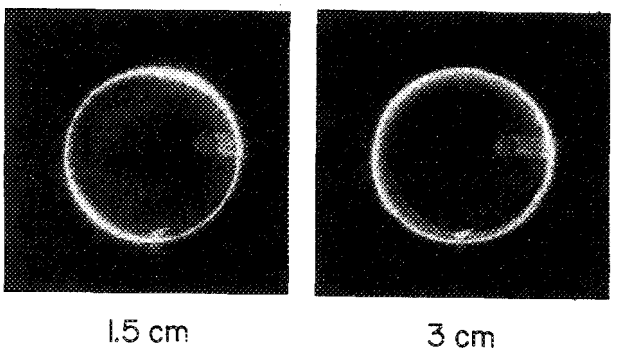

FIG. 6. Photographs of the beam cross section at several axial positions in the downstream field for the case $V = 26$ kV, $\alpha = \beta_\theta/\beta_z = 2$, and $\Omega/\gamma = 2\pi \times 875$ MHz.

streaming, hollow, nonrotating electron beam is emitted from a thermionic cathode Pierce-type electron gun, and the sharp radial magnetic field at the cusp transition produces a $v_z \times B_r$ force which results in axis-encircling Larmor orbits downstream with reduced axial velocity. The thermionic cathode has an inner radius of 1.4 cm, outer radius of 1.6 cm, and is located 4.9 cm from the anode surface which is a stainless-steel plate attached to the iron plate. To avoid background gas charge neutralization of the beam, the gun is pulsed for 3 μs at a repetition rate of 60 Hz with typical beam voltage 27 kV and current 1.0 A. The solenoids that produce the cusp field are operated dc with magnetic field magnitudes typically in the range 300–400 G.

There are four solenoid coils in the Maryland experiment, two upstream and two downstream. The field for each coil in the presence of the intervening iron plate was measured independently and linear superposition using a short computer program adjusts the strength of each coil to obtain an optimal cusp. Figure 5 shows the measured optimum axial magnetic field at the beam radius $r_0 = 1.5$ cm with effective transition width $\zeta = 4.8$ mm.

A fluorescent screen in the downstream vacuum chamber was used to measure inner and outer radii as a function of axial position. Shown in Fig. 6 are frames of the first few positions, moving downstream from the iron plate for the case $V = 26$ kV, $\alpha = \beta_\theta/\beta_z = 2$, and $\Omega/\gamma = 2\pi \times 875$ MHz. The first frame was taken with zero applied magnetic field to provide a reference with respect to beam rotation. Given the measured value of ζ, Eqs. (5) and (6) yield $r_{gc} = 2.7$ mm for the guiding-center radius and $\lambda = 4.72$ cm for the scallop wavelength. Plotted in Fig. 7 is the beam envelope from fluorescent screen data yielding measured values $r_{gc} = 3.2 \pm 0.5$ mm and $\lambda = 5.5 \pm 0.6$ cm, which agrees fairly well with theory considering thermal velocity spreads and space charge were not taken into account.

Magnetic cusp technology has improved considerably since the design and construction of the present experiment. For example, a small "bump" on the axial magnetic field profile immediately before and after the cusp transition counteracts the effect of a finite transition width, greatly reducing the magnitude of coherent off-centering.[29,30] And the spread in axial velocities due to the spread in canonical

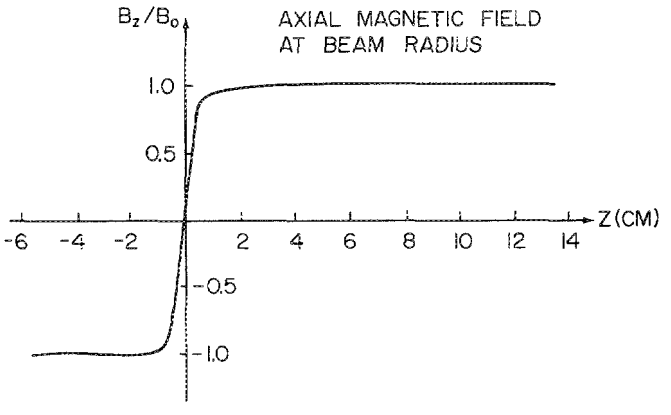

FIG. 5. Measured optimum axial magnetic field at the beam radius $r_0 = 1.5$ cm. Effective transition width $\zeta = 4.8$ mm [Eq. (4)].

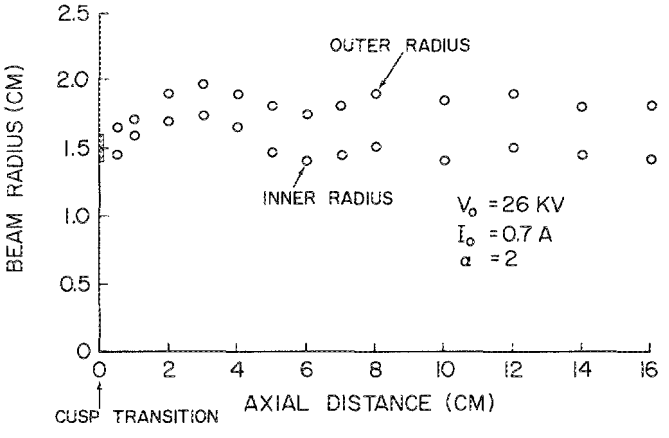

FIG. 7. Beam envelope from fluorescent screen data yielding measured values $r_{gc} = 3.2 \pm 0.5$ mm and $\lambda = 5.5 \pm 0.6$ cm.

angular momentum can be reduced by post-cusp beam-compression techniques.[31] Most importantly, these improvements can be made while preserving the simplicity of a Pierce-type planar diode gun, making cusp-injected systems very attractive for devices requiring annular rotating electron beams.

III. MICROWAVES

The magnetronlike microwave cavities used in the high-harmonic experiments are, in general, capable of operating at many frequencies. In sufficiently tenuous beams, the oscillation frequency will be near one of the normal modes (cold cavity) of the structure. Considered here is only this condition, which is denoted resonant interaction.

If the resonant mode spacings are sufficiently large, then mode control is achievable because the beam-microwave interaction is a function of the applied magnetic field. There are (at least) two classes of rotating-beam–microwave interactions relevant to this experiment that can result in growth of an electromagnetic wave. In the first case, the beam and the wave rotate at the same rate so that each electron sees approximately a constant field. This interaction is denoted synchronous. For axis-encircling electron orbits (large orbit gyrotron) the interaction results in azimuthal density bunching, whereas electrons with off-axis orbits (gyrotron) become phase synchronized. If operation is designed for the l_0th harmonic, then the synchronous condition is $\omega = l_0(\Omega/\gamma)$ in the nonrotating inertial beam frame, where ω is the electromagnetic wave frequency and Ω/γ is the relativistic cyclotron frequency. The second case is characterized by $\omega = (l_0 - 1)\Omega/\gamma$ (also in the beam frame), which implies that in one revolution each electron traverses a full sinusoidal period of the electromagnetic wave. This interaction is called a cyclotron mode and related devices are called peniotrons.[32,33]

Linear perturbations on beams synchronized with the electromagnetic wave generally grow faster than perturbations on beams experiencing variations at the cyclotron frequency [e.g., see Eq. (20) of Ref. 34] and so the synchronous growth rates are usually higher, although theoretical studies have predicted extremely high efficiencies ($\gtrsim 90\%$) for cyclotron mode devices.[33] The microwave circuits described here are designed to operate in the resonant, synchronous (or large orbit gyrotron) mode based on a previously derived growth rate formula.[17] The idealized beam model and large orbit gyrotron growth rate formula are briefly discussed below followed by the main experimental results of the low-energy device at Maryland.

A. Theory

The model for the electron beam in the microwave circuit is shown in Fig. 8. The unperturbed beam is assumed to be thin and cold, i.e., all electrons have the same Larmor radius r_0, guiding-center radius $r_{gc} = 0$, and velocity distribution $(0, c\beta_{\theta_0}, c\beta_{z_0})$ where c is the velocity of light. The beam's intensity is characterized by Budker's parameter $\nu = n_s e^2 r_0 \mu_0/(2m_0)$ where n_s is the surface density of electrons, e and m_0 are the charge magnitude and rest mass of an electron, and μ_0 is the permittivity of free space. The beam

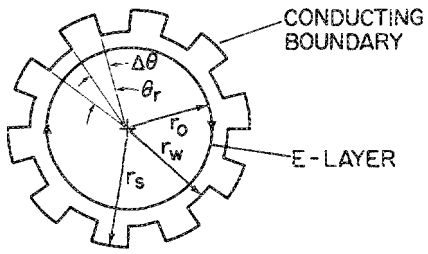

FIG. 8. Cross section of slotted-wall magnetron structure and circulating E layer.

propagates down a long magnetron structure which is immersed in a uniform magnetic field of magnitude B_0. The vane structure has n slots, with azimuthal walls defined by constant radii and radial walls defined by constant angles. The inner radius is denoted r_w, the outer radius r_s, the angular slot opening $\Delta\theta$, and angle of one period $\theta_r = 2\pi/n$. We assume that there are $1 \leqslant l_0 \leqslant n$ beam bunches.

Because of the aximuthally periodic wall structure, cold-cavity modes generally contain all azimuthal harmonics. For relatively small slot openings ($\Delta\theta/\theta_r \leqslant 0.5$), it is reasonable to assume that the fields in the slots ($r_w < r < r_s$) contain only the lowest harmonic.[35,36] This implies that magnetron-TE modes have constant fields across slot openings and that adjacent (slot) resonators have fields that differ only by a constant phase ($2\pi l_0/n$). In the interaction region ($r < r_w$), the nonzero harmonics are given by $l_0 + qn$, where q is an integer.

The approximate cold-cavity dispersion relation for the magnetron-TE modes[18,35] is given by $D(\xi) = 0$, where

$$D(\xi) = \frac{J_0(x_w)Y_0'(x_s) - Y_0(x_w)J_0'(x_s)}{J_0'(x_w)Y_0'(x_s) - Y_0'(x_w)J_0'(x_s)} - \left(\frac{\Delta\theta}{\theta_r}\right)\sum_{q=-\infty}^{+\infty}\frac{J_{l_0+qn}(x_w)}{J'_{l_0+qn}(x_w)} \times\left(\frac{\sin[(l_0+qn)\Delta\theta/2]}{(l_0+qn)\Delta\theta/2}\right)^2, \tag{7}$$

$\xi = [(\omega/c)^2 - k_z^2]^{1/2}$ (k_z is the axial wave number), $x = r\xi$, $x_w = r_w\xi$, $x_s = r_s\xi$, and J_0 and Y_0 are Bessel functions of the first and second kinds. Because the dispersion relation depends only on ξ, the solutions are hyperbolas in the ω-k_z plane. Furthermore, the waveguide mode based on harmonic l_0 has the same cutoff frequency as the mode based on harmonic $n - l_0$. Considered here is only the lowest radial mode; thus modes are labeled exclusively by their azimuthal content with acknowledgment of the abovementioned degeneracy in the following manner: $(l_0, n - l_0)$. In this notation, the 2π mode would be labeled $(n,0)$ and the π mode $(n/2,n/2)$. The cold-cavity TE modes for the waveguide structure of Table II are illustrated in Fig. 9. The modes are fairly well spread and all higher-order radial modes are above 11 GHz.

The microwave signal grows from noise via the resonant interaction between the beam and the azimuthal electric field of the l_0th harmonic of the electromagnetic wave. Energy is coupled to the other harmonics through the slots. To lowest order, the beam perturbation lies on the surface de-

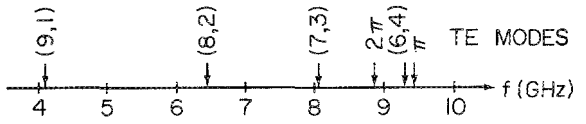

FIG. 9. Cold-cavity TE-mode cutoff frequencies for slotted-wall structure of Table II.

fined by $r = r_0$. The beam-wave dispersion relation is found by writing the perturbed electron trajectories in terms of the local electromagnetic fields and closing the equations by estimating the "jump" in the fields across the electron sheet. The resultant growth rate at a resonant axial wave number is given by[18]

$$\frac{\Gamma}{\Omega/\gamma} = \frac{\sqrt{3}}{2}\left[\frac{2\nu/\gamma}{x_w(\Omega/\gamma)\partial_\omega D(\xi)}\left(\frac{\Delta\theta}{\theta_r}\right)\right. \times\left.\left(\frac{\sin(l_0\Delta\theta/2)}{l_0\Delta\theta/2}\right)^2\left(\frac{x_0 J_{l_0}'(x_0)}{J_{l_0}'(x_w)}\right)^2\right]^{1/3}. \quad (8)$$

The growth rates for the beam and waveguide parameters of Table II are shown in Fig. 10. The beam current is taken to be 1.5 A which gives a surface density $n_s = 2.5\times10^{12}\ \mathrm{m}^{-2}$. The beam energy is adjusted slightly to give a nearly tangential intersection (grazing condition) between the tenth-harmonic beam line and the 2π-mode dispersion curve at 8.91 GHz. The growth rates for the (8,2) mode synchronous intersections at 6.73 and 7.53 GHz are slightly greater than the 2π mode, and the (9,1) mode growth rates at 7.08 and 8.96 GHz are down by about a factor of 3.

B. Experiment

The large orbit gyrotron beam-injection system is as described in Sec. II B. In the downstream vacuum chamber the various slotted-wall magnetron structures are held in place by support rings. The slots are tapered on the input side of the multiresonator structure. The axial lengths of the structures are on the order of 30 cm with a 1-cm gap between the abruptly ending slotted waveguide and a glass output window.

Microwave output power is collected by an X-band standard gain horn positioned at the output window. The signal is sent through a directional coupler and rotary vane attenuator to a detector and spectrum analyzer. The receiving horn aperture encompasses the slotted-wall waveguide diameter; however, cold-cavity tests have shown that less than 10% of the output power couples to the receiving horn. Poor conversion from the cylindrical magnetron modes to the rectangular waveguide TE_{01} mode is the main reason for the low coupling coefficient. Since cold-cavity testing of this type is an inaccurate process and the downstream beam current is not measured directly, large error bars are placed on total power measurements and corresponding efficiencies, typically $\pm$ 3 dB.

Significant microwave power was obtained from this tube operating as an oscillator in several distinct modes. There were cases where different modes were excited simultaneously; however, by tuning the magnetic field and particle energy it was possible to operate in a single mode. Reported here will be the main results obtained from testing three different slotted-wall magnetron structures.

The first two structures were designed to operate under similar beam conditions at the tenth cyclotron harmonic, one in the 2π mode and the other in the π mode. The motivation for this is to compare threshold beam power required for oscillation in the two modes, since the theoretical treatment of Chu and Dialetis predicts that the π mode has a lower threshold than the 2π mode.[23] The structures were manufactured by stamping out a corrugated sheet of 10-mil stainless-steel foil and then wrapping it upon itself to form a cylindrical slotted-wall structure as shown in Fig. 8. Spot welding and support rings hold it in place inside the vacuum chamber. The dimensional tolerances and mechanical uniformity of the two structures turned out to be poor, $\pm$ 0.02 in. in wall radius and slot depth. Table I contains the dimensions and operating parameters of the two structures.

Total output microwave power and efficiency for the

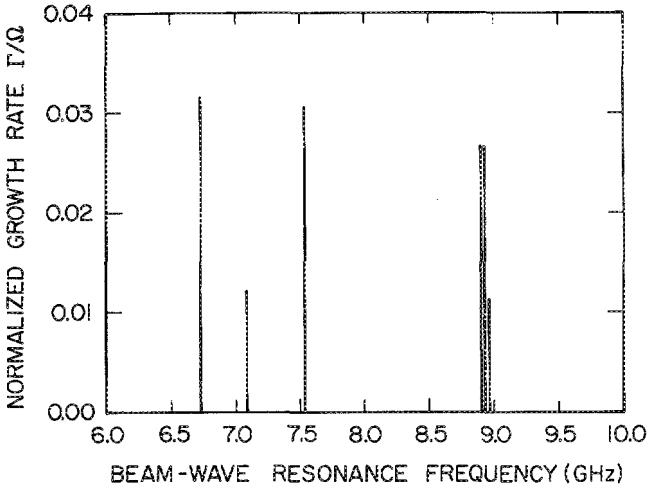

FIG. 10. Linear growth rates for the beam and waveguide parameters of Table II. Only synchronous resonances are considered. The growth rates at 8.91 GHz are for grazing condition resonance between the 2π waveguide mode and the tenth-harmonic beam line. Growth rates at 6.73 and 7.53 GHz are for the (8,2) mode interacting with the eighth-harmonic beam line and the growth rates at 7.08 and 8.96 GHz are for the (9,1) mode interacting with the ninth-harmonic beam line.

TABLE I. Dimensions and operating parameters for the π- and 2π-mode stainless-steel magnetron structures.

	π structure	2π structure
Number of slots	20	10
Radius r_w (cm)	1.9	2.0
Radius r_s (cm)	2.53	2.47
$\Delta\theta/\theta_r$	0.5	0.5
Axial length (cm)	24.5	27.7
Cutoff frequency (GHz)	8.83	7.79
Operating frequency (GHz)	8.91	7.93
Beam energy (keV)	26	26
Nominal beam radius (cm)	1.5	1.5
Relativistic cyclotron frequency (MHz)	875	772
Compression ratio β_θ/β_z	2	1.25

two structures were low, $P_\mu \approx 10$ W and $\eta \approx 0.1\%$, but their relative performances qualitatively agreed with theory. Plotted in Fig. 11 is total microwave power versus input beam current at a fixed beam energy. Obviously the π-mode structure has a significantly lower threshold beam power than the 2π-mode structure. Because there has been no quantitative analysis with respect to threshold beam power and diffractive Q for the two structures, it has not been possible to deduce cavity Q's given measured threshold power.[23]

The third magnetron structure tested had ten slots and performed well in the 2π mode at the tenth cyclotron harmonic and in the (8,2) mode at the eighth cyclotron harmonic. It was initially designed to operate in the 2π mode with beam and waveguide parameters listed in Table II. The structure was manufactured by an electroforming process whereby an aluminum mandril is machined to very close tolerances, placed in a copper sulfate electrolytic solution where pure copper deposits onto the mandril, followed by acid etching of the aluminum. The result is a pure copper magnetron structure with wall thickness $\sim 1/16$ in. and dimensional tolerances of ± 0.001 in. The time-integrated, multiple-shot frequency measurements for this structure were taken with a Hewlett-Packard HP-8569B spectrum analyzer from which it was possible to identify resonances at specific waveguide modes. Even though the structure was designed to operate at the tenth-harmonic 2π mode, the eighth-harmonic (8,2) mode was also a possible mode of operation.

Shown in Fig. 12 is the ω-k diagram for TE modes present in the ten-slot waveguide along with the eighth cyclotron harmonic beam line which includes the expected dispersion in particle velocity. The dotted line represents the observed microwave frequency of 6.78 GHz, corresponding to the voltage pulse, detector response, and spectrum analyzer traces shown in Fig. 13. This (8,2) mode interacting with the eighth cyclotron harmonic was the most powerful obtained, having an instantaneous power of 9.1 ± 5.2 kW with efficiency $42\% \pm 24\%$ at beam energy 27 keV and current 0.8 A. The resonant instability appears to be the backward wave given by the beam-waveguide intersection of Fig. 12. The fact that the signal tuned in with sharp dependence on particle energy and magnetic field is another confirmation of backward-wave resonance. The measured linewidth was very narrow, 5 MHz full width at half maximum (FWHM) on a 6.78-GHz center line which includes shot-to-shot variation.

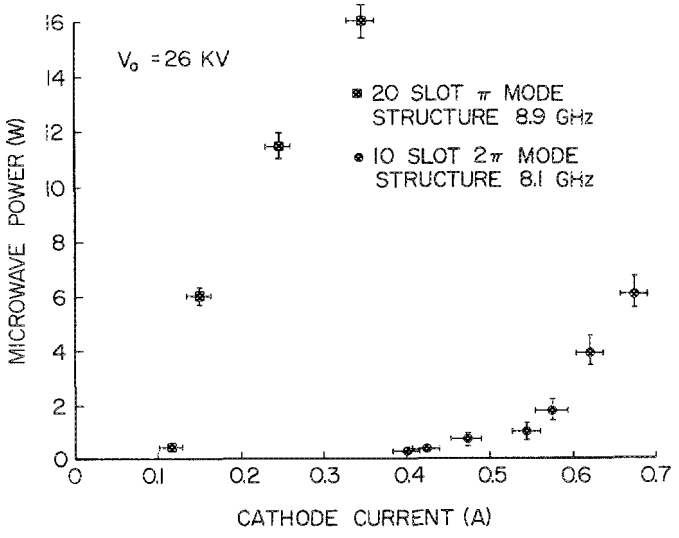

FIG. 11. Total microwave power vs input beam current at a fixed beam energy for a π-mode structure and a 2π-mode structure.

TABLE II. Dimensions and operating parameters for the 2π-mode copper magnetron structure.

Number of slots	10
Radius r_w (cm)	1.8
Radius r_s (cm)	2.19
$\Delta\theta/\theta_r$	0.5
Axial length (cm)	24.5
Cutoff frequency (GHz)	8.83
Operating frequency (GHz)	8.91
Beam energy (keV)	26
Nominal beam radius (cm)	1.5
Relativistic cyclotron frequency (MHz)	875
Compression ratio β_θ/β_z	2

The other mode producing significant power was the tenth-harmonic 2π mode at 8.85 GHz. The ω-k diagram with the tenth-harmonic beam line is shown in Fig. 14, the dotted line again representing observed frequency. This mode had an instantaneous power of 2.2 ± 1.3 kW, corresponding to an efficiency of $14\% \pm 8\%$ for beam energy 28 keV and current 0.56 A. Voltage pulse, detector response, and spectrum analyzer traces are shown in Fig. 15 from which it can be seen that the 2π resonance is not as pure as the (8,2) resonance of Fig. 13. However, the spurious modes accompanying the 2π resonance are down by > 35 dB. The linewidth was again very narrow, 4 MHz on an 8.85-GHz center line.

IV. CONCLUSIONS

Experimental modes of operation of a low-energy large orbit gyrotron microwave tube have been identified. The

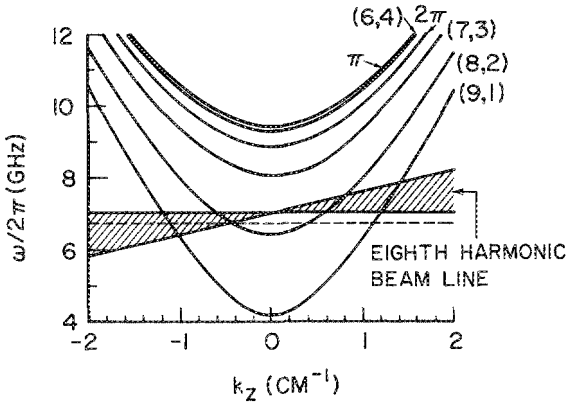

FIG. 12. ω-k diagram for TE modes present in the ten-slot waveguide along with the eighth cyclotron harmonic beam line which includes expected dispersion in particle velocity. The dotted line represents the observed microwave frequency of 6.78 GHz.

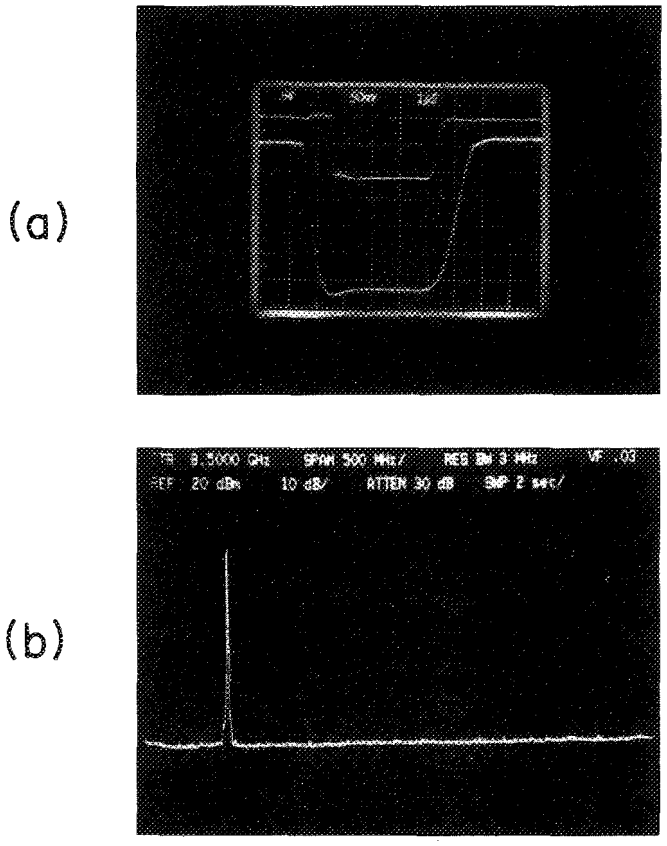

FIG. 13. (a) Detector response (top) and voltage pulse (bottom, 5 kV per division) and (b) spectrum analyzer trace for the (8,2) mode excitation. Instantaneous microwave power 9.1 ± 5.2 kW at 6.78 GHz with efficiency 42% ± 24% at 27 keV and 0.8 A.

(8,2) mode at the eighth cyclotron harmonic and the 2π mode at the tenth cyclotron harmonic produced power in the kW range corresponding to efficiencies of tens of percent. Plots of beam perturbation modes superimposed on electromagnetic waveguide dispersion curves verify the microwave-generating mechanism as the synchronous electron cyclotron maser instability; i.e., a mode requiring l_0 azimuthal density bunches produced radiation at the l_0th cyclotron harmonic. The dominance of the (8,2) mode and the 2π mode over the (9,1) mode is consistent with calculated linear growth rates.

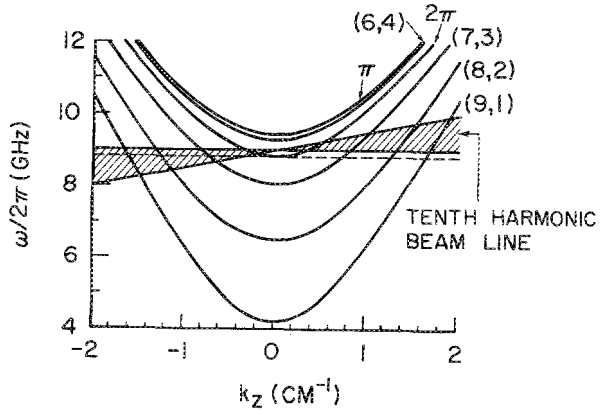

FIG. 14. ω-k diagram with tenth-harmonic beam line. The dotted line represents the observed microwave frequency of 8.85 GHz.

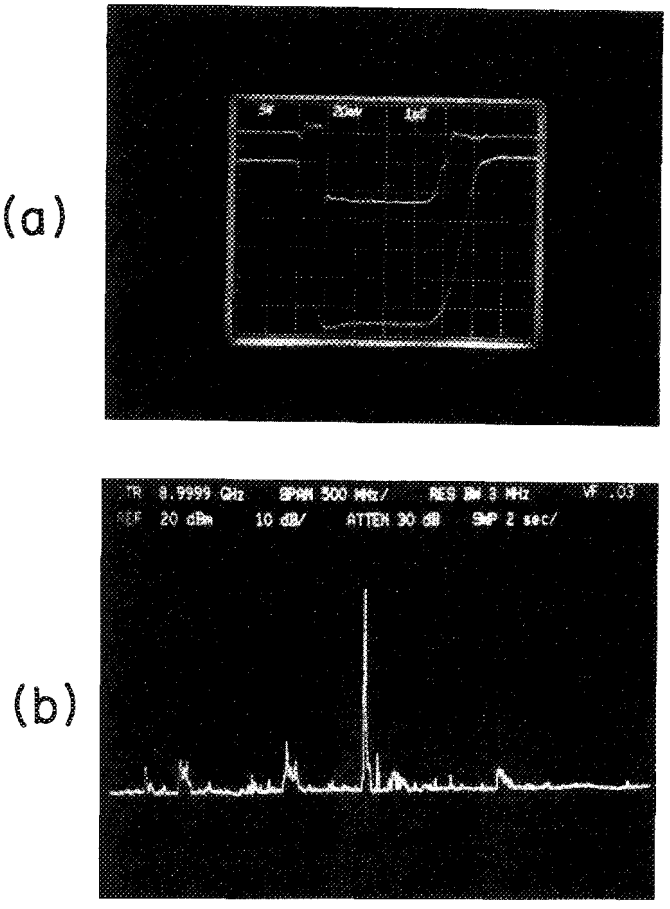

FIG. 15. (a) Detector response (top) and voltage pulse (bottom, 5 kV per division) and (b) and spectrum analyzer trace for the 2π-mode excitation. Instantaneous microwave power 2.2 ± 1.32 kW at 8.85 GHz with efficiency 14% ± 8% at 28 keV and 0.56 A.

Experimental results qualitatively agree with the theoretical prediction that the beam current threshold for start oscillation is lower for the π mode than for the 2π mode. Some uncertainty in this conclusion still exists, however, given the overall poor performance of the two structures compared and that the beam parameters for the two cases were different.

Having demonstrated the feasibility and principle of operation of the large orbit gyrotron at both mildly relativistic and extremely relativistic energies, experiments are being pursued which explore other ranges of operation in power and frequency as well as operation of the device in an amplifier mode. A necessary development in future devices will be an efficient method of power extraction. Possible methods are a small antenna inserted into the waveguide[35] or coupling a rectangular waveguide to one or more of the slot resonators as is done in magnetrons.

ACKNOWLEDGMENTS

We are grateful to C. D. Striffler for many helpful discussions and suggestions. This work was supported by the Air Force Office of Scientific Research and the U. S. Department of Energy.

[1]V. A. Flyagin, A. V. Gapanov, M. I. Petelin, and V. K. Yulpatov, IEEE Trans. Microwave Theory Tech. **MTT-25**, 514 (1977).
[2]J. L. Hirschfield and V. L. Granatstein, IEEE Trans. Microwave Theory Tech. **MTT-25**, 528 (1977).
[3]H. S. Uhm, R. C. Davidson, and K. R. Chu, Phys. Fluids **21**, 1877 (1978).
[4]N. M. Kroll and W. A. McMullin, Phys. Rev. A **17**, 300 (1978).
[5]P. Sprangle, R. A. Smith, and V. L. Granatstein, in *Infrared and Submillimeter Waves*, edited by K. Button (Academic, New York, 1979), Vol. 1, p. 279, and references therein.
[6]W. A. McMullin and G. Bekefi, Appl. Phys. Lett. **39**, 845 (1981).
[7]R. A. Mahaffey, P. Sprangle, J. Golden, and C. A. Kapetanakos, Phys. Rev. Lett. **39**, 843 (1977).
[8]H. E. Brandt, A. Bromborsky, H. B. Bruns, and R. A. Kehs, in *Proceedings of the 2nd International Topical Conference on High Power Electron Ion Beam Research Technology* (Cornell University, Ithaca, NY, 1977), Vol. 11, p. 649.
[9]A. Palevsky and G. Bekefi, Phys. Fluids **22**, 986 (1979).
[10]T. J. Orzechowski and G. Bekefi, Phys. Fluids **22**, 978 (1979).
[11]Y. Carmel and J. A. Nation, J. Appl. Phys. **44**, 5268 (1973).
[12]R. A. Kehs, Y. C. Carmel, and M. C. Wang, IEEE Trans. Plasma Sci. **PS-13**, 559 (1985).
[13]W. W. Destler, R. L. Weiler, and C. D. Striffler, Appl. Phys. Lett. **38**, 570 (1981).
[14]C. D. Striffler, W. W. Destler, R. Kulkarni, and R. L. Weiler, IEEE Trans. Nucl. Sci. **NS-30**, 3429 (1983).
[15]W. W. Destler, R. Kulkarni, C. D. Striffler, and R. L. Weiler, J. Appl. Phys. **54**, 4152 (1983).
[16]W. Namkung, Phys. Fluids **27**, 329 (1984).
[17]W. Lawson and C. D. Striffler, Phys. Fluids **28**, 2868 (1985).
[18]W. Lawson, W. W. Destler, and C. D. Striffler, IEEE Trans. Plasma Sci. **PS-13**, 444 (1985).
[19]W. W. Destler, D. W. Hudgings, M. J. Rhee, S. Kawasaki, and V. L. Granatstein, J. Appl. Phys. **48**, 3291 (1977).
[20]W. W. Destler, H. Romero, C. D. Striffler, R. L. Weiler, and W. Namkung, J. Appl. Phys. **52**, 2740 (1981).
[21]Y. Y. Lau and L. R. Barnett, Int. J. Infrared Millimeter Waves **3**, 619 (1982).
[22]H. S. Uhm, C. M. Kim, and W. Namkung, Phys. Fluids **27**, 488 (1984).
[23]K. R. Chu and D. Dialetis, Int. J. Infrared Millimeter Waves **5**, 37 (1984).
[24]J. Y. Choe and W. Namkung, IEEE Trans. Nucl. Sci. **NS-32**, 2882 (1985).
[25]W. Namkung and J. Y. Choe, IEEE Trans. Nucl. Sci. **NS-32**, 2885 (1985).
[26]M. J. Rhee and W. W. Destler, Phys. Fluids **17**, 1574 (1974).
[27]G. Schmidt, Phys. Fluids **5**, 994 (1962).
[28]J. Sinnis and G. Schmidt, Phys. Fluids **6**, 841 (1963).
[29]G. P. Scheitrum and R. True, Tech. Dig.—Int. Electron Devices Meet. **81**, 332 (1981).
[30]M. Reiser, University of Maryland Electron Ring Accelerator Technical Note 76-004 (1976).
[31]W. Lawson and P. E. Latham, J. Appl. Phys. **61**, 519 (1986).
[32]P. Sprangle, J. Appl. Phys. **47**, 2935 (1976).
[33]P. Vitello and K. Ko, IEEE Trans. Plasma Sci. **PS-13**, 454 (1985).
[34]W. Lawson and C. D. Striffler, Phys. Fluids **29**, 1682 (1986).
[35]G. B. Collins, *Microwave Magnetrons*, MIT Radiation Laboratory Series (McGraw-Hill, New York, 1948).
[36]J. Y. Choe, Bull. Am. Phys. Soc. **28**, 1142 (1983).